MATERIALS CHEMISTRY
FRONTIERS

RESEARCH ARTICLE

View Article Online
View Journal | View Issue

Cite this: *Mater. Chem. Front.*, 2018, **2**, 718

Electron-transporting foldable alternating copolymers of perylenediimide and flexible macromolecular chains†

Tsuneaki Sakurai, *[a] Naomi Orito,[a] Shusaku Nagano,[b] Kenichi Kato,[c] Masaki Takata[c] and Shu Seki *[a]

Tuning the electrical conductivity of conjugated macromolecules by nanostructure ordering plays a key role in developing carrier transporting materials applicable to flexible organic electronic devices. Alternating copolymers of perylene-3,4,9,10-tetracarboxylic acid diimide (PDI) and flexible macromonomers, poly(dimethylsiloxane) (PDMS), poly(ethylene glycol) (PEG), or poly(propylene glycol) (PPG), were synthesized *via* simple polycondensation reactions between 3,4,9,10-perylenetetracarboxylic dianhydride (PTCDA) and bis-amine-terminated corresponding macromonomers. Dynamic traces of absorption and fluorescence spectra of the series of alternating copolymers, with the indication of PDI chromophores, suggested the more foldable nature in tetrahydrofuran of the PDMS-based polymer than of the PEG- and PPG-based polymers. The folding capability of these polymers in solution was confirmed by fluorescence spectra and the absolute fluorescence quantum efficiency values. In the solid films, the condensed state of the polymers showed X-ray diffraction patterns of periodic structures, which depend on the type of macromolecular chains: PEG showed a highly crystallized state in contrast to the slightly crystalline PDI molecules in the PDMS and PPG-based polymers. Photoconductivity upon ultraviolet excitation has been screened by noncontact microwave measurements, and the mobility of electrons has also been characterized based on the kinetic traces of radical anions on the PDI chromophores. The negligible optical absorption observed from the PDMS-based polymers revealed the lowest photocarrier generation yield among the prepared polymers. The observed low conductivity for the PDMS-based, most foldable polymers possibly results from a lower photo-charge generation yield and thermal fluctuations of the flexible PDMS chains. The PEG-based polymer marked the largest electron mobility of 0.2 $cm^2\ V^{-1}\ s^{-1}$, reflecting the highly crystalline nature of the PEG chains.

Received 28th December 2017,
Accepted 31st January 2018

DOI: 10.1039/c7qm00616k

rsc.li/frontiers-materials

Introduction

Materials available for flexible electronics have attracted increasing attention in recent years, and polymer-based materials have played a key role in the devices.[1–4] Flexible and solution-processable polymers for electronics are often composed of π-conjugated segments and flexible insulated chains, where the former relies on electrical conductivity and the latter secures flexibility and solubility. Among the explored polymer electronics, block copolymers containing π-conjugated molecules are interesting motifs because they are known to form micrometer–nanometer domains *via* self-assembly to afford directional charge transport properties.[5,6] There, the flexible segments not only work as solubilizing parts but also allow nanostructure-directing functions. On the other hand, alternating polymers (oligomers) of π-conjugated molecules and insulated flexible chains (a kind of multi-block copolymer) have not been fully explored toward organic electronics, though they have the potential to construct one- or two-dimensional arrays of π-electronic systems *via* intrapolymer folding[7] and/or interpolymer π–π interactions. Flexible, and even elastic characters would be added to those alternating copolymers if the entropic spring of macromolecular chains was utilized.

Liquid crystal polymers[8] are a representative class of such rigid–flexible alternating copolymers that has been studied before. In its early stage, mesogenic behaviors and the nanostructure of mesogens and linkers were studied, where the mesogenic parts

[a] *Department of Molecular Engineering, Graduate School of Engineering, Kyoto University, Nishikyo-ku, Kyoto 615-8510, Japan. E-mail: sakurai-t@moleng.kyoto-u.ac.jp, seki@moleng.kyoto-u.ac.jp*
[b] *Nagoya University Venture Business Laboratory, Nagoya University, Furo-cho, Chikusa, Nagoya 464-8603, Japan*
[c] *Materials Visualization Photon Science Group, RIKEN SPring-8 Center, 1-1-1 Kouto, Sayo, Hyogo, 679-5148, Japan*

† Electronic supplementary information (ESI) available: Dynamic light scattering data and differential scanning calorimetry chart. See DOI: 10.1039/c7qm00616k

were mostly composed of phenylene- or oligophenylene- based molecular units while alkyl or oligo(ethylene glycol) (OEG) chains were used as flexible linkers.[9–13] Then, molecular arrangements or supramolecular structures of rigid–flexible alternating copolymers attracted attention for tuning of their photophysical properties.[14] For example, photoluminescence and electroluminescence were realized for rod–coil copolymers from oligo(*p*-phenylene vinylene)s and alkyl chains.[15–18] Although the structural information in their solid states is still difficult to clarify, material application as a solid-state emitter was clearly demonstrated.

From the viewpoint of solution-state assembly, rigid–flexible polymers (oligomers) have been studied within the concept of a ''foldamer''. A foldamer is initially defined as ''any polymer with a strong tendency to adopt a specific, compact conformation'',[19,20] which features hydrogen bonding-assisted helical or sheet-like folding behaviors that mimic biomacromolecules like proteins. Afterwards, another definition was proposed: ''Any oligomer that folds into a conformationally ordered state in solution, the structures of which are stabilized by a collection of noncovalent interactions between nonadjacent monomer units'',[21,22] highlighting that the cooperative interactions include various interactions such as π–π and hydrophobic ones. Recently, other types of folding polymers have been broadly interpreted as foldamers. Multi-block copolymers of π-conjugated rods and hydrophilic chains were utilized for biomimetic applications in their folded forms.[23,24] Another interesting feature in recent reports is the integration into two-dimensional nanosheets from the pre-organized folded crystallization assembly of rigid–flexible alternating polymers/oligomers in solution.[25–27] Namely, the macroscopic assembly of foldable polymers[25–28] provides the potential for soft materials to be used in their solid-state.

Based on the above background, we have started to evaluate the intrinsic charge carrier transport property of foldamer systems. Foldable polyurethanes carrying naphthalene diimides as side groups[29] and thiophene nanosheets from alternating co-oligomers of bithiophene and oligo(ethyleneglycol) units[30] were previously studied by the flash-photolysis time-resolved microwave conductivity (FP-TRMC) technique, a contactless microwave-based evaluation method of photo-generated charge carriers.[31–33] In the present work, our attention is given to the characterization of charge transport properties of simple rod–coil foldamer systems. Perylene-3,4,9,10-tetracarboxylic acid diimide (PDI) was chosen as a rod-shaped π-system because PDI is known to show strong π–π interactions.[34] Most of the reported foldamers employ hydrogen bonds or crystallization of aromatic segments without strong π–π interactions. Main-chain liquid crystals also usually involve mesogens that cannot stack on each other in a solution state. We consider that strong π–π interactions of PDIs would result in the folded assembly in solution when PDIs are linked with flexible macromolecular chains. The cast films from these assemblies will eventually provide electron transport pathways. So far, alternating copolymers[35–38] and co-oligomers[39–42] of a PDI derivative and flexible chain were reported by several groups. No obvious folding behavior was confirmed in solution for those of PDI and macromonomers,[35–38] while folding behaviors of the above discrete oligomers were investigated in detail.[39–42] However, none of them focused on their semiconducting and photoconductive properties. Here, we chose amine-terminated poly(dimethylsiloxane) (PDMS), poly(ethylene glycol) (PEG) and poly(propylene glycol) (PPG) as flexible macromonomer chains, and conjugated them with 3,4,9,10-perylenetetracarboxylic dianhydride *via* polycondensation reactions (Scheme 1). The resulting PDI–flexible chain multi-block copolymers were studied in solution and film states. We revealed that folding behaviors in solution were drastically changed depending on the type of linker chain. In solid films, the intrinsic electron mobility along stacked PDI units, estimated by the FP-TRMC technique, was found to reach up to 0.2 $cm^2\ V^{-1}\ s^{-1}$.

Experimental

Materials

3,4,9,10-Perylenetetracarboxylic dianhydride (PTCDA) and quinoline were purchased from Tokyo Chemical Industry Co. Tetrahydrofuran (THF), chloroform ($CHCl_3$), and $Zn(OAc)_2$ were purchased from Wako Pure Chemical Industries. Poly(dimethylsiloxane), bis(3-aminopropyl) terminated (average $M_n \sim 2\,500$), poly(propylene glycol)bis(2-aminopropyl ether) (average $M_n \sim 2000$ and 4000), poly(ethylene glycol)diamine (average $M_n \sim 2000$ and 6000), and methoxy poly(ethylene glycol)amine (average $M_n \sim 2000$, extent of labelling: >0.4 mmol g^{-1} NH_2 loading) were purchased from Sigma-Aldrich. Aminopropyl terminated polydimethylsiloxane (average $M_n \sim 1000$ and 5000) and monoaminopropyl terminated poly(dimethylsiloxane) (average $M_n \sim 2000$) were purchased from Gelest.

Measurements and methods

Molecular weights of polymers were determined by size exclusion chromatography (SEC) with polystyrene standards. SEC analysis was performed on HITACHI model L-2130, L-2455, L-2530 chromatography instruments with Shodex KF-804L/KF-805L columns using THF as an eluent at a flow rate of 1 mL min^{-1} at 40 °C. A refractive index detector and multi-wavelength photodiode array detector were used for detecting the elution peaks. Polymerization progress was confirmed by the analytical SEC at 520 nm absorption after 24 h of reaction. The crude polymers were purified by recycling preparative HPLC on a Japan Analytical Industry Co. model LC-9210NEXT equipped with JAIGEL-2.5HH/-3HH columns. Electronic absorption spectra were recorded on a JASCO model V-570 UV/VIS/NIR spectrophotometer. The variable-temperature measurements were carried out using a screw-cap quartz cuvette. Photoluminescence spectra were recorded on a HITACHI model F-2700 spectrofluorometer. Absolute photoluminescence quantum yield was evaluated on a Hamamatsu model Quantaurus-QY absolute PL quantum yield measurement system. Dynamic light scattering was measured on a Malvern model Zetasizer system. Powder X-ray diffraction measurements were carried out using a synchrotron radiation X-ray beam with a wavelength of 0.108 nm on BL44B2[43] at the Super Photon Ring (SPring-8, Hyogo, Japan). A large Debye–Scherrer camera was used in conjunction with an

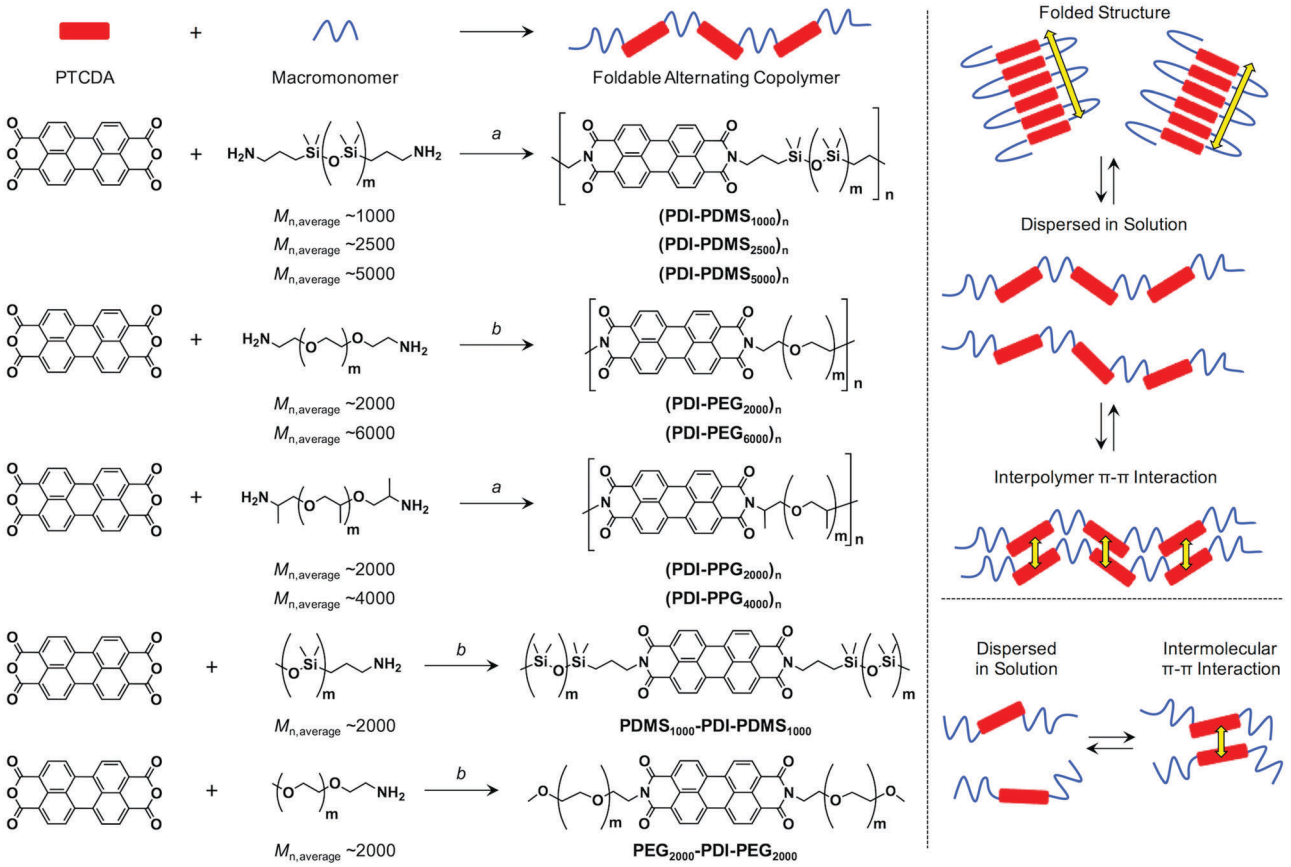

Scheme 1 (left) Synthetic schemes of PDI–flexible chain alternating copolymers and reference compounds. (a) Imidazole, 200 °C, 24 h; (b) imidazole, $Zn(OAc)_2$, quinoline, 200 °C, 24 h. (right) Schematic illustration of possible patterns of intra/inter-polymer/molecular π–π interactions among PDI units for PDI–flexible chain polymers and reference compounds.

imaging plate as a detector, and all diffraction patterns were recorded with a 0.01° step in 2θ. During the measurements, samples were put into a 0.5 mm thick glass capillary and rotated to obtain a homogeneous diffraction pattern. The exposure time to the X-ray beam was 1.5 min. Grazing-incidence X-ray scattering (GIXS) measurements for the cast films were performed using a Rigaku FR-E X-ray diffractometer with a Rigaku model R-AXIS IV 2D detector.[44] Cu Kα radiation (λ = 0.1542 nm) with a beam size of approximately 300 μm × 300 μm was used for the X-ray beams, while the camera length was set at 300 mm. The sample stage was composed of a goniometer and vertical stage (CHUO Precision Industria ATS-C316-EM/ALV-300-HM). Flash-photolysis time-resolved microwave conductivity (FP-TRMC) measurements were carried out at 25 °C in air with a resonant cavity. The resonant frequency and power of the microwave probes were 9.1 GHz and 3 mW, respectively. Charge carriers were photo-injected into the sample upon exposure to a third harmonic generation (λ = 355 nm) of a Spectra Physics model INDI-HG Nd:YAG laser with a pulse duration of 5–8 ns. The photon density of the 355 nm laser pulse was 9.1×10^{15} photons cm^{-2}. The TRMC signal picked up by a diode (rise time < 1 ns) was monitored by a Tektronics model TDS3052B digital oscilloscope. The observed conductivities, given by the photo-carrier generation yield (ϕ) multiplied by the sum of charge carrier mobilities ($\sum\mu$), were normalized according to the equation;

$$\phi \sum \mu = \frac{1}{eAI_0F}\frac{\Delta P_r}{P_r}. \quad (1)$$

where, e, A, I_0, F, P_r, and ΔP_r represent unit charge of a single electron, sensitivity factor (S^{-1} cm), incident photon density of the excitation laser (photon cm^{-2}), filling factor (cm^{-1}), and reflected microwave power and its change, respectively. The value of F was calculated based on the optical density depth profiles and geometry of the samples overlapped to the electric field strength E in the cavity as,

$$F = \alpha \ln 10 \int 10^{-\alpha} E^2 dx dy dx / \int E^2 dx dy dx \quad (2)$$

where α is the absorptivity of the sample, giving the value of F as $1.0–1.2 \times 10^3$ cm^{-1} for all the prepared dropcast film samples. Transient absorption spectroscopy (TAS) measurements were carried out at 25 °C in air. The photon density of a λ = 355 nm pulse was 9.1×10^{15} photons cm^{-2}. A white-light continuum from a Xe lamp was used as a probe-light source for TAS. The monochromated probe light was guided into a wide-dynamic-range streak camera system (Hamamatsu C7700), which collected

a two-dimensional image of the spectral and temporal profiles of light intensity.

Synthesis of alternating copolymers and reference polymers

Condition A. PTCDA (40 mg, 100 μmol, 5 eq.) and macromonomer (20 μmol, 1 eq.) were added to imidazole (100 mg, 1.47 mmol), and the resulting mixture was stirred at 200 °C for 24 h under a N_2 atmosphere. After cooling down to room temperature, the reaction mixture was extracted with toluene, washed with water (×3), dried over Na_2SO_4, and evaporated to dryness. The residue was dissolved in $CHCl_3$ and purified by preparative SEC on JAIGEL-2.5HH/3HH columns using $CHCl_3$ as an eluent.

Condition B. PTCDA (29 mg, 72 μmol, 1 eq.), macromonomer (72 μmol, 1 eq.), imidazole (100 mg, 1.47 mmol), and $Zn(OAc)_2 \cdot 2H_2O$ (12 mg, 55 μmol) were added to quinoline (4.0 mL), and the resulting mixture was stirred at 200 °C for 24 h under a N_2 atmosphere. After cooling down to room temperature, MeOH was added and the precipitate was collected. The residue was dissolved in $CHCl_3$ and purified by preparative SEC on JAIGEL-2.5HH/3HH columns using $CHCl_3$ as an eluent.

Condition C. PTCDA (9.48 mg, 12.0 μmol, 1 eq.), macromonomer (24.0 μmol, 2 eq.), imidazole (50.0 mg) and $Zn(OAc)_2 \cdot 2H_2O$ (3.0 mg, 14 μmol) were added to quinolone (1.3 mL), and the resulting mixture was stirred at 200 °C for 24 h under a N_2 atmosphere. After cooling down to room temperature, MeOH was added and the precipitate was collected. The residue was dissolved in $CHCl_3$ and purified by preparative SEC on JAIGEL-2.5HH/3HH columns using $CHCl_3$ as an eluent.

Synthesis of $(PDI–PDMS_{1000})_n$. By using condition A, aminopropyl terminated polydimethylsiloxane (average $M_n \sim 1000$) and PTCDA were polymerized and purified. $M_n = 44 \times 10^3$ g mol^{-1}, $M_w = 82 \times 10^3$ g mol^{-1}, polydispersity index: $Đ = 1.9$.

Synthesis of $(PDI–PDMS_{2500})_n$. By using condition A, poly(dimethylsiloxane), bis(3-aminopropyl) terminated (average $M_n \sim 2500$) and PTCDA were polymerized and purified. $M_n = 54 \times 10^3$ g mol^{-1}, $M_w = 88 \times 10^3$ g mol^{-1}, polydispersity index: $Đ = 1.6$.

Synthesis of $(PDI–PDMS_{5000})_n$. By using condition A, aminopropyl terminated polydimethylsiloxane (average $M_n \sim 5000$) and PTCDA were polymerized and purified. $M_n = 25 \times 10^3$ g mol^{-1}, $M_w = 74 \times 10^3$ g mol^{-1}, polydispersity index: $Đ = 3.0$.

Synthesis of $(PDI–PEG_{2000})_n$. By using condition B, poly(ethylene glycol)diamine (average $M_n \sim 2000$) and PTCDA were polymerized and purified. $M_n = 7 \times 10^3$ g mol^{-1}, $M_w = 8 \times 10^3$ g mol^{-1}, polydispersity index: $Đ = 1.1$.

Synthesis of $(PDI–PEG_{6000})_n$. By using condition B with a modification (using 5 eq. PDCTA instead of 1 eq.), poly(ethylene glycol)diamine (average $M_n \sim 6000$) and PTCDA were polymerized and purified. $M_n = 8 \times 10^3$ g mol^{-1}, $M_w = 12 \times 10^3$ g mol^{-1}, polydispersity index: $Đ = 1.6$.

Synthesis of $(PDI–PPG_{2000})_n$. By using condition A with a modification (using 8 eq. PTCDA instead of 5 eq.), poly(propylene glycol)bis(2-aminopropyl ether) (average $M_n \sim 2000$) and PTCDA were polymerized and purified. $M_n = 32 \times 10^3$ g mol^{-1}, $M_w = 56 \times 10^3$ g mol^{-1}, polydispersity index: $Đ = 1.7$.

Synthesis of $(PDI–PPG_{4000})_n$. By using condition A, poly(propylene glycol)bis(2-aminopropyl ether) (average $M_n \sim 4000$) and PTCDA were polymerized and purified. $M_n = 12 \times 10^3$ g mol^{-1}, $M_w = 23 \times 10^3$ g mol^{-1}, polydispersity index: $Đ = 1.8$.

Synthesis of $(PDMS_{2000}–PDI–PDMS_{2000})_n$. By using condition C, monoaminopropyl terminated poly(dimethylsiloxane) (average $M_n \sim 2000$) and PTCDA were reacted and purified. $M_n = 1.0 \times 10^3$ g mol^{-1}, $M_w = 1.4 \times 10^3$ g mol^{-1}, polydispersity index: $Đ = 1.4$.

Synthesis of $(PEG_{2000}–PDI–PEG_{2000})_n$. By using condition C, methoxy poly(ethylene glycol)amine (average $M_n \sim 2000$, extent of labelling: >0.4 mmol g^{-1} NH_2 loading) and PTCDA were reacted and purified. $M_n = 4.8 \times 10^3$ g mol^{-1}, $M_w = 5.4 \times 10^3$ g mol^{-1}, polydispersity index: $Đ = 1.1$.

Results and discussion

Design of rod–coil foldable alternating copolymers

The driving force of the folding event for a polymer has been well discussed and rationalized in terms of the loss of the conformational entropy in the folded state with its much larger conformational ensemble and the enthalpic gains.[22] In other words, folding requires less reduction in entropy than the process of intermolecular self-assembly, and thus folding is favoured in solution interpreted by the second law of thermodynamics. The enthalpic gain is mainly given by the π–π interactions for π-conjugated units, which motivated us to use PDI molecules capable of strong association capability. The enthalpic gains on folding and interpolymer interaction between two PDI units should be almost identical ($\Delta H_{fold} \sim \Delta H_{self\text{-}assembly} < 0$) because the stacking geometry of two PDI units should be the same. However, the entropic changes on folding and interpolymer self-assembly are quite different. According to a simple model,[41] we can conclude that the entropic loss is larger for interpolymer self-assembly ($\Delta S_{fold} < \Delta S_{self\text{-}assembly} < 0$). Therefore, a folding process is much favored compared with interpolymer self-assembly. If the enthalpic gain exceeds entropic loss at that temperature, folding must take place. As introduced above, PDI units were previously incorporated in rod (PDI)–coil (flexible macromolecular chains) alternating polymers but distinguished folding behaviors in solution were not observed for these polymers.[35–38] It is assumed that the used polymeric linkers such as poly(tetrahydrofuran) do not have high enough flexibility for the small entropic losses. On the other hand, Li *et al.* found that PDI–oligo(ethylene glycol) (OEG) oligomers fold in solution,[39–42] which indicates that the short and flexible linker of OEG helps the folded structure to be stable at the temperature and concentration. Again, none of these examples addressed the charge transport property given by stacked PDI arrays.

Aiming for compatibility of simple synthesis and facile film fabrication capability, a condensation reaction between 3,4,9,10-perylenetetracarboxylic dianhydride (PTCDA) and an amine-terminated flexible macromonomer was employed to form an imide bond, which constructs the main chains for these polymers (Scheme 1). In order to suppress the entropy loss, we chose highly flexible poly(dimethylsiloxane) (PDMS)

chain as macromonomers.[45–47] This flexibility relies on the long Si–O bond, as well as a small rotational barrier along Si–O–Si (~3.3 kJ mol^{-1} around a Me_2Si–O bond) and variability of its bond angle.[48] In addition, poly(ethylene glycol) (PEG) and poly(propylene glycol) (PPG) were also studied, taking into account their more flexible nature than long alkyl and poly(tetrahydrofuran) chains due to the high content of C–O–C bonds with similar character[49] to the Si–O–Si bond.

Synthesis of foldable alternating copolymers

According to the Experimental section, PTCDA and amine-terminated macromonomers (7 types: Scheme 1) were polymerized at 200 °C in molten imidazole or a quinoline solution of imidazole and $Zn(OAc)_2$, both of which are typically used for the conversion from PTCDA to a PDI derivative.[34] Since amine-terminated PDMSs and PPGs are liquid or fluidic even at room temperature, the polymerization was carried out in molten imidazole. In the case with amine-terminated PEGs, the macromonomers are solid and thus the reactions were carried out in quinoline solution. After polymerization for 24 h, imidazole and $Zn(OAc)_2$ were removed from the mixtures, which were eventually purified by preparative size-exclusion chromatography (SEC) using crosslinked polystyrene beads, where the high-molecular weight fraction was collected as $CHCl_3$ solutions. The molecular weight was estimated by analytical SEC using THF as an eluent with polystyrene standards. As discussed later, some of the obtained alternating copolymers are considered to be folded in THF. In that sense, the absolute values of number-average molecular weight (M_n) and weight-average molecular weight (M_w) with respect to polystyrene standards cannot be simply used for determining the degree of polymerization (n). However, the analytical SEC results summarized in Table 1 suggested that PEG-based foldamers have small molecular weights while those with PDMS or PPG were much more elongated. This fact can be understood because the initial PEG macromonomers are not fluidic but solid and their solubility is not good, resulting in the faster precipitation during polymerization reactions even though quinoline solvent was added. Moreover, the theoretically preferred molar ratios of PTCDA and macromonomers are 1 : 1 for copolymers and 1 : 2 for reference macromonomers. However, we found that a larger amount of PTCDA (*e.g.* 5 eq. to the macromonomer) resulted in the observation of higher molecular-weight polymers in analytical SEC. Thus, we chose the reaction conditions as described in Table 1. In fact, PTCDA cannot be completely soluble in quinoline or molten imidazole, which may be the reason for the unbalanced molar ratios affording relatively high molecular weight polymers.

Folding behaviors in solution

The folding behaviors of the prepared polymers were primarily monitored by absorption spectra of PDI chromophores as a probe in solution.[41,42] It is known that PDI-based cyclophanes[50,51] and folded[39–42]/self-assembled[52,53] PDI chromophores with H-aggregation mode[54] have an inverse intensity distribution among their vibronic states, $A^{0\rightarrow0}/A^{0\rightarrow1} < 1$, whereas dissociated PDI molecules have usual Franck–Condon progressions with $A^{0\rightarrow0}/A^{0\rightarrow1} \sim 1.6$.[55] Therefore, the absorption ratio of the 0 → 0 (*ca.* 530 nm) to 0 → 1 (*ca.* 490 nm) transitions can be used, as long as no concentration dependence is observed, to briefly quantify the degree of folding in the PDI-containing polymers. This remarkable intensity reversal originates from the strong electron–phonon coupling in PDI dimers as the absorption maximum blue shifts by *ca.* 0.17 eV from the 0 → 0 transition to the 0 → 1 transition. As discussed previously,[41,42] the relative intensities of the vibronic bands for PDI molecules are dominated by the Franck–Condon factors. The intensity reversal indicates that the optimum overlap has shifted from (0 → 0, $\langle\chi_{v=0}'|\chi_{v=0}\rangle$) in free monomers to (0 → 1, $\langle\chi_{v=1}'|\chi_{v=0}\rangle$) in the π-staked structures, where χ and χ' are the ground- and excited-state vibronic wave functions, respectively. The strong electron–phonon coupling indicates that the PDI molecules adopt a largely eclipsed H-stacking structure with π–π distances less than the van der Waals contact to establish quantum interactions of π-orbital overlaps.

Table 1 Summary of reaction conditions, average molecular weights M_n and M_w, and polydispersity index $Đ$ for PDI-based alternating copolymers and reference compounds

Entry	Reaction condition[a]	Monomer ratio[b]	M_n/g mol^{-1}	M_w/g mol^{-1}	$Đ$
(PDI–PDMS$_{1000}$)$_n$	A	5	44×10^3	82×10^3	1.9
(PDI–PDMS$_{2500}$)$_n$	A	5	54×10^3	88×10^3	1.6
(PDI–PDMS$_{5000}$)$_n$	A	5	25×10^3	74×10^3	3.0
(PDI–PEG$_{2000}$)$_n$	B	1	7.0×10^3	8.0×10^3	1.1
(PDI–PEG$_{6000}$)$_n$	B	8	8.0×10^3	12×10^3	1.6
(PDI–PPG$_{2000}$)$_n$	A	8	32×10^3	56×10^3	1.7
(PDI–PPG$_{4000}$)$_n$	A	8	12×10^3	23×10^3	1.8
PDMS$_{2000}$–PDI–PDMS$_{2000}$	C	0.5	1×10^3	1.4×10^3	1.4
PEG$_{2000}$–PDI–PEG$_{2000}$	C	0.5	4.8×10^3	5.4×10^3	1.1

[a] See synthesis in Experimental section. [b] Molar ratio of the PTCDA/macromonomer.

As shown in Fig. 1, **(PDI–PDMS$_{1000}$)$_n$** and **(PDI–PDMS$_{2500}$)$_n$** in THF exhibited inverse intensity distributions of $A^{0\rightarrow0}/A^{0\rightarrow1}$ (α) = 0.62 and 0.59, respectively. These values are quite small, which is indicative of strong π–π interactions among the PDI chromophores. In contrast, $CHCl_3$ and toluene solutions of these polymers showed different spectral patterns. **(PDI–PDMS$_{1000}$)$_n$** in $CHCl_3$ and toluene yielded the α values of 0.97 and 0.95, respectively, which were obviously larger than that in THF. For **(PDI–PDMS$_{2500}$)$_n$**, the α values are still lower than 1; 0.78 in $CHCl_3$ and 0.74 in toluene. **(PDI–PDMS$_{5000}$)$_n$** has higher solubility than the above two polymers most likely because it has relatively large PDMS segments, leading to the fact that it was soluble even in hexane (α = 0.89). However, still, THF was found to be the most effective solvent to induce π–π interactions among PDI chromophores in solution (Fig. 1c), where the α value was calculated to be 0.62. Then, other polymers were investigated in the same manner. **(PDI–PEG$_{2000}$)$_n$** showed an inverse intensity distribution with $A^{0\rightarrow0}/A^{0\rightarrow1}$($\alpha$) = 0.90 in THF, while the spectral shape indicated the presence of completely dissociated PDI chromophores in $CHCl_3$ (Fig. 1d). By changing the average M_n of PEG chains from 2000 to 6000, the spectral patterns in THF and toluene represent normal intensity distributions (Fig. 1e). Namely, chain length is

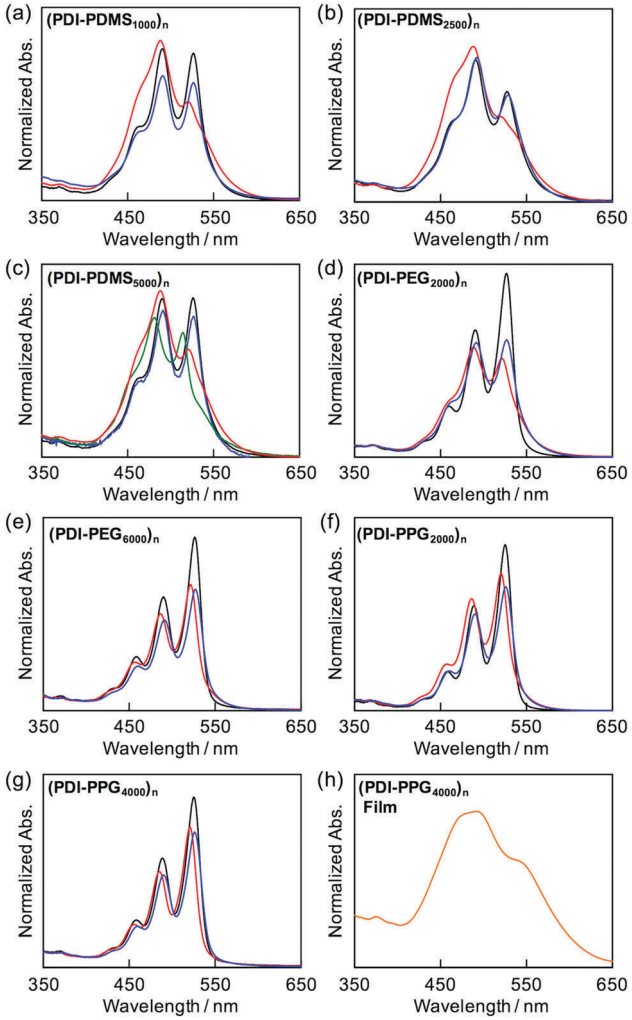

Fig. 1 Absorption spectra of (a) **(PDI–PDMS$_{1000}$)$_n$**, (b) **(PDI–PDMS$_{2500}$)$_n$**, (c) **(PDI–PDMS$_{5000}$)$_n$**, (d) **(PDI–PEG$_{2000}$)$_n$**, (e) **(PDI–PEG$_{6000}$)$_n$**, (f) **(PDI–PPG$_{2000}$)$_n$**, and (g) **(PDI–PPG$_{4000}$)$_n$** at 10^{-4} M in $CHCl_3$ (black), THF (red), toluene (blue), and *n*-hexane (green). (h) Absorption spectra of spincoated film of **(PDI–PPG$_{4000}$)$_n$**.

an important parameter for the folding event, as initially expected due to entropic factors. For the PPG-based copolymers, both **(PDI–PPG$_{2000}$)$_n$** and **(PDI–PPG$_{4000}$)$_n$** in all three solvents displayed absorption spectra with a normal intensity distribution (Fig. 1f and g). This might be due to hampering by the branched methyl groups of propylene glycol chains next to the nitrogen atoms of imide groups (Scheme 1),[56,57] leading to the suppression of the folding behaviour. To address the quantitative contribution from entropy loss in the folding behaviour, temperature-dependent absorption spectra were measured for representative foldable polymers, **(PDI–PDMS$_{5000}$)$_n$** and **(PDI–PEG$_{2000}$)$_n$**, as shown in Fig. 2a–c.[58] Partial dissociation of PDI stacks in the folded state was clearly observed both in THF (Fig. 2a) and toluene (Fig. 2b), whereas there is only a little change in good solvent at the same concentration (Fig. S1, ESI†). It should be noted that the dissociation was observed in the identical temperature range despite the different solvation enthalpies between THF and toluene, suggesting the dissociation behavior originates primarily from the entropy gain in PDMS chains. A similar tendency was confirmed for **(PDI–PEG$_{2000}$)$_n$** in toluene (Fig. 2c). Based on the absorption intensity plots at different wavelengths (Fig. S2, ESI†), it can be concluded that the observed temperature dependence was different from a simple association/dissociation model often used for PDI compounds[52,53] and reflected more complicated processes. However, the fact that the α values became larger upon heating suggests the progression of the dissociation. Importantly, the absorption spectra were independent of the concentration of polymers in these solvents at 10^{-6}–10^{-4} M (Fig. 2d–f). According to the association constants of PDIs in solutions usually falling in the range around 10^2–10^3 M^{-1},[57] concentration-dependent stacking behaviours should appear at these concentration ranges. However, in the present case, the spectral patterns in THF explicitly indicate PDI–PDI interactions even in the highly-diluted solutions (monomer-unit concentration: 10^{-6} M), and thus all the spectral

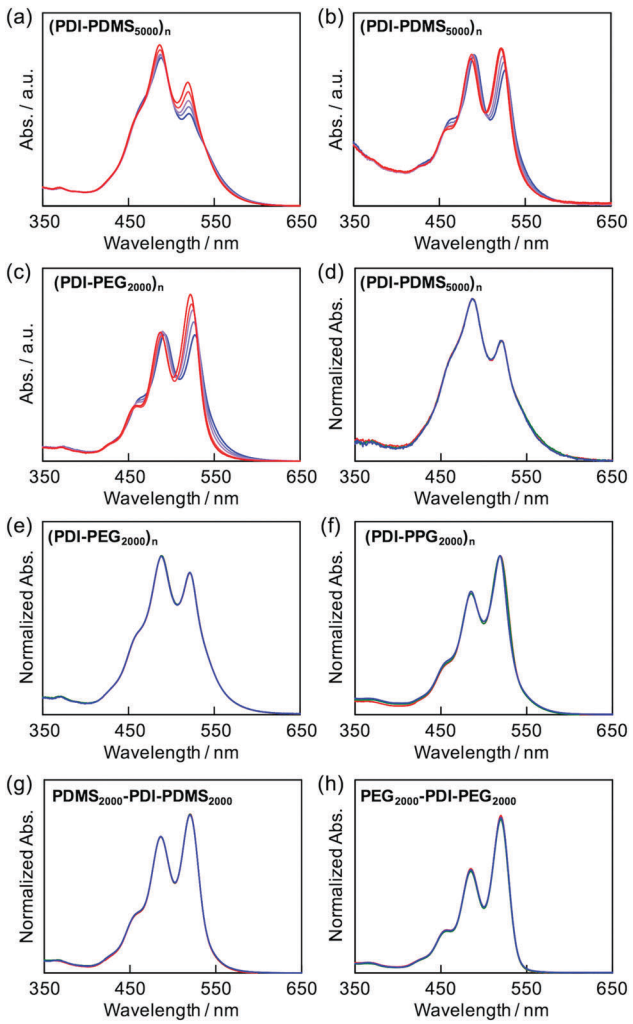

Fig. 2 Variable-temperature absorption spectra of (a) **(PDI–PDMS$_{5000}$)$_n$** in THF at 10^{-5} M from 20 °C (blue) to 60 °C (red) at every 10 °C, (b) **(PDI–PDMS$_{5000}$)$_n$** in toluene at 10^{-5} M from 20 °C (blue) to 100 °C (red) at every 10 °C, and (c) **(PDI–PEG$_{2000}$)$_n$** in toluene at 10^{-5} M from 20 °C (blue) to 100 °C (red) at every 20 °C. Absorption spectra of (d) **(PDI–PDMS$_{5000}$)$_n$**, (e) **(PDI–PEG$_{2000}$)$_n$**, (f) **(PDI–PPG$_{2000}$)$_n$**, (g) **PDMS$_{2000}$–PDI–PDMS$_{2000}$**, and (h) **PEG$_{2000}$–PDI–PEG$_{200}$** in THF at 10^{-6} M (red), 10^{-5} M (green), and 10^{-4} M (blue).

changes in Fig. 1 primarily relate to folding/unfolding events of isolated macromolecular chains containing interactions among multi-PDI chromophores.

The folding capability of the **(PDI–PDMS$_m$)$_n$** series and **(PDI–PEG$_{2000}$)$_n$** is also supported indirectly by the spectral changes observed in the reference macromonomer compounds of **PDMS$_{2000}$–PDI–PDMS$_{2000}$** and **PEG$_{2000}$–PDI–PEG$_{2000}$**, as seen in Fig. 2g and h. Up to the concentration of 10^{-4} M, no characteristic spectral change was observed, indicating no concentration dependence of inter-PDI interactions. Moreover, the values of α for these compounds in THF were estimated to be 1.22 and 1.59, which correspond to normal intensity distributions between $A^{0\rightarrow0}$ and $A^{0\rightarrow1}$. Interconversion of the normal/inverse intensity distributions, depending on solvents, was specifically observed for the polymers. This suggests that the PDI aggregations take place only in the folded state of the polymers. It should be noted that dynamic light scattering measurements of polymers in solutions also suggested the dispersed, non-aggregated state of the polymers (Fig. S3, ESI†).

Relationship between folding and emission property

The stacking nature of PDIs in the folded states could also be investigated by fluorescence spectroscopy for all the prepared

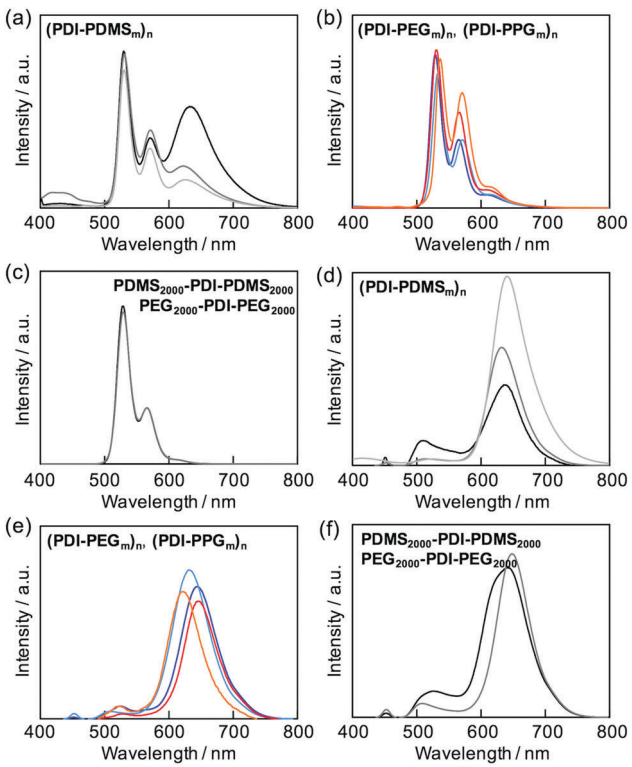

Fig. 3 Emission spectra of (a) **(PDI–PDMS$_{1000}$)$_n$** (black), **(PDI–PDMS$_{2500}$)$_n$** (gray), and **(PDI–PDMS$_{5000}$)$_n$** (light gray), (b) **(PDI–PEG$_{2000}$)$_n$** (blue), **(PDI–PEG$_{6000}$)$_n$** (light blue), **(PDI–PPG$_{2000}$)$_n$** (red), and **(PDI–PPG$_{4000}$)$_n$** (orange), and (c) **PDMS$_{2000}$–PDI–PDMS$_{2000}$** (black) and **PEG$_{2000}$–PDI–PEG$_{2000}$** (gray) in THF at 10^{-5} M. Emission spectra of (d) **(PDI–PDMS$_{1000}$)$_n$** (black), **(PDI–PDMS$_{2500}$)$_n$** (gray), and **(PDI–PDMS$_{5000}$)$_n$** (light gray), (e) **(PDI–PEG$_{2000}$)$_n$** (blue), **(PDI–PEG$_{6000}$)$_n$** (light blue), **(PDI–PPG$_{2000}$)$_n$** (red), and **(PDI–PPG$_{4000}$)$_n$** (orange), and (f) **PDMS$_{2000}$–PDI–PDMS$_{2000}$** (black) and **PEG$_{2000}$–PDI–PEG$_{2000}$** (gray) in solid films.

Table 2 Summary of absolute emission quantum efficiency in THF at 10^{-5} M. λ_{ex} = 450 nm

Entry	Φ	$A^{0\rightarrow0}/A^{0\rightarrow1}$
(PDI–POMS$_{2500}$)$_n$	0.23	0.59
(PDI–PDMS$_{5000}$)$_n$	0.30	0.65
(PDI–PEG$_{2000}$)$_n$	0.32	0.89
(PDI–PEG$_{6000}$)$_n$	0.59	1.30
(PDI–PPG$_{2000}$)$_n$	0.38	1.22
(PDI–PPG$_{4000}$)$_n$	0.52	1.36
PDMS$_{2000}$–PDI–PDMS$_{2000}$	0.48	1.22
PEG$_{2000}$–PDI–PEG$_{2000}$	0.76	1.59

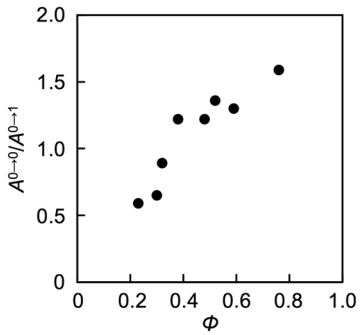

Fig. 4 Plots of absolute quantum efficiency Φ and the ratio of absorption intensity $A^{0\rightarrow0}/A^{0\rightarrow1}$ (=α) of PDI chromophores in THF. Φ and α values are extracted from Table 2.

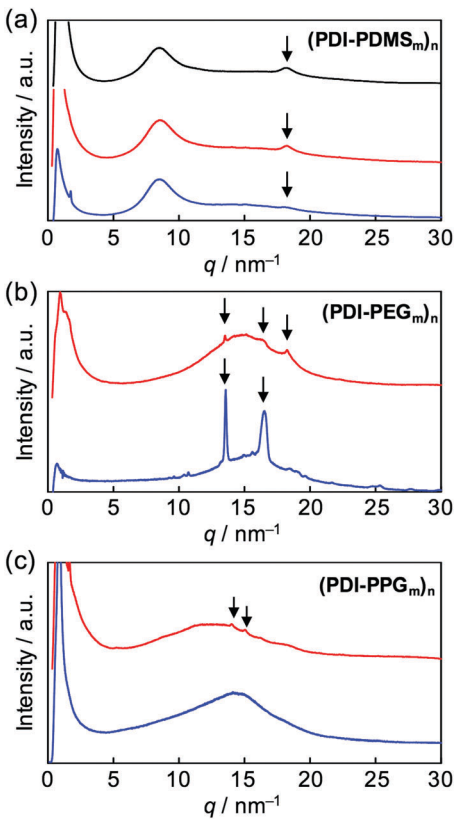

Fig. 5 Powder X-ray diffraction patterns of (a) **(PDI–PDMS$_{1000}$)$_n$** (black), **(PDI–PDMS$_{2500}$)$_n$** (red), and **(PDI–PDMS$_{5000}$)$_n$** (blue), (b) **(PDI–PEG$_{2000}$)$_n$** (red) and **(PDI–PEG$_{6000}$)$_n$** (blue), and (c) **(PDI–PPG$_{2000}$)$_n$** (red) and **(PDI–PPG$_{4000}$)$_n$** (blue).

polymers. Most of the polymers exhibited fluorescence originating from a singlet excited state of isolated PDIs in the corresponding macromolecular chains (Fig. 3b). The two macromonomer compounds also followed this tendency (Fig. 3c). The only exceptional case was observed for the **(PDI–PDMS$_m$)$_n$** series, giving a clear structureless emission band at around 630 nm (Fig. 3a); a characteristic peak of excimer emission.[34,59] The relative intensity of the emission bands depended on the flexible PDMS length; the shorter chains allowed effective formation of PDI aggregates in the excited state.

In the condensed phases, all of the polymers showed almost complete suppression of emission from isolated PDI molecules, and the emission was converted into that of excimers (Fig. 3d–f). This implies that the flexible chains of PDMS, PEG, and PPG are not able to completely hamper aggregations among PDIs, and the excited energy relaxation occurs *via* intermolecular energy transfer among PDIs in the solid state.

Aggregation-induced quenching of excited energies on PDI molecules can be discussed quantitatively by the emission quantum efficiency, as summarized in Table 2. The quantum efficiency of a reference macromonomer, **PEG$_{2000}$–PDI–PEG$_{2000}$**, reached Φ = 0.76 in THF, which almost corresponds to the efficiency from free PDI molecules in nonpolar solvents.[34,57,60] However, the value considerably drops down to Φ = 0.48 for the other reference macromonomer, **PDMS$_{2000}$–PDI–PDMS$_{2000}$**. This is most likely due to the vibrational coupling between PDI cores and PDMS chains with much higher flexibility at room temperature, providing non-radiative pathways of excited energy dissipation. In contrast to the high quantum efficiencies of the above reference compounds, the values were obviously lower in the polymers, particularly in the ones with the shorter flexible chains. PDMS-based copolymers were revealed to show especially low quantum yields, which is consistent not only with their excimer formation capability (Fig. 3a) but also with their effective aggregation tendency in THF (Fig. 1a–c). The interesting relationship is the positive correlation between the values of Φ and α (Fig. 4). Both absorption and fluorescence spectral studies disclosed the validity of the alternating copolymer design with large π-conjugated cores and flexible macromolecular chains. Based on the reported glass transition temperature T_g of PDMS (~ -120 °C),[61] PEG (~ -60 °C),[62] PPG (~ -70 °C)[63] chains with sufficient molecular weights, the most flexible nature of the PDMS chains is reasonable and it accounts for the relatively-favored folding structures from the viewpoint of entropy. Although the T_g of PPG is the second-lowest, the stacking of PDI units may be restricted by the branched methyl groups of propylene units,[56,57] resulting in the unfolded behaviour. PEG-based copolymers serve as a foldamer depending on the PEG linker length that plays an important role in the entropy term.

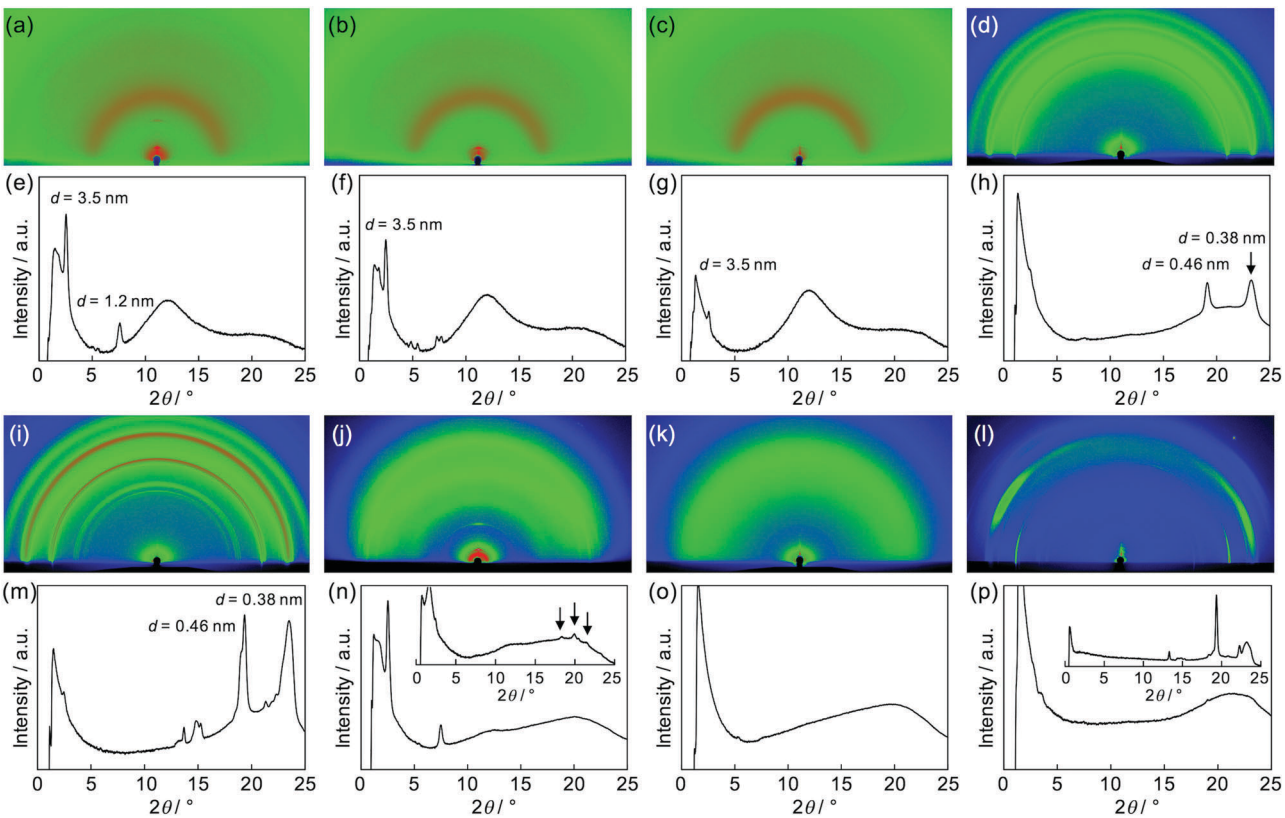

Fig. 6 Two-dimensional images of X-ray scattering measurements for cast films of (a) **(PDI–PDMS$_{1000}$)$_n$**, (b) **(PDI–PDMS$_{2500}$)$_n$**, (c) **(PDI–PDMS$_{5000}$)$_n$**, (d) **(PDI–PEG$_{2000}$)$_n$**, (i) **(PDI–PEG$_{6000}$)$_n$**, (j) **(PDI–PPG$_{2000}$)$_n$**, (k) **(PDI–PPG$_{4000}$)$_n$**, and (l) **PEG$_{2000}$–PDI–PEG$_{2000}$**. ((e–h) and (m–p)) Out-of-plane scattering profiles of the corresponding GIXS images ((a–d) and (i–l)). Insets in (n) and (p) show in-plane scattering profiles.

Self-organized behaviors in solid states

After the confirmation of the folding behaviours in solution, self-assembly of these polymers in solid states was investigated. Differential scanning calorimetry traces, exemplified for **(PDI–PDMS$_{5000}$)$_n$** (Fig. S4, ESI†), indicated no remarkable phase transition from −50 to 300 °C. Then, X-ray diffraction (XRD) analysis at room temperature was attempted. Powder XRD measurements for non-oriented samples were carried out and one-dimensional diffraction patterns were obtained, as shown in Fig. 5. The polymers of the **(PDI–PDMS$_m$)$_n$** series provided broad peaks at around q = 9 and 18 nm^{-1} (Fig. 5a). The former is derived from loose packings of PDMS chains while the latter may be PDI–PDI spacings. The spacing values of the latter peaks were calculated as d = 3.35 Å, corresponding to the inter-plane distance of stacking PDI systems.[64] **(PDI–PEG$_m$)$_n$** polymers showed one broad diffraction at *ca.* q = 15 nm^{-1} (Fig. 5b), which likely results from an amorphous halo of PEG chains. However, a set of sharp crystalline peaks (q ∼ 13–18 nm^{-1}) was also observed for the PEG-based polymers, in particular for **(PDI–PEG$_{6000}$)$_n$**. Crystallization was more facilitated for longer PEG chains, whereas the peak at d = 3.42 Å was also observed for **(PDI–PEG$_{2000}$)$_n$**. For PPG-based polymers, only **(PDI–PPG$_{2000}$)$_n$** implied the presence of crystalline peaks (Fig. 5c). Considering the amorphous feature for the pattern of **(PDI–PPG$_{4000}$)$_n$**, the slight crystalline character may be related to the packing of PDI units. The pattern of **(PDI–PPG$_{2000}$)$_n$** contains a broad peak at d = 3.38 Å.

Then, as can be seen in Fig. 6, grazing-incidence X-ray scattering (GIXS) two-dimensional images were obtained for the dropcast films of these polymers from THF solutions on a quartz substrate. Apparently, crystallization of PEG chains in the **(PDI–PEG$_{2000}$)$_n$** and **(PDI–PEG$_{6000}$)$_n$** films was characterized with particularly strong peaks at d = 0.38 and 0.46 nm (Fig. 6h and m). Meanwhile, the amorphous character of **(PDI–PPG$_{4000}$)$_n$** was again confirmed (Fig. 6o). For **(PDI–PPG$_{2000}$)$_n$**, anisotropic structural ordering was observed (Fig. 6n). While crystalline peaks appeared in the in-plane direction similar to its powder XRD pattern, two scattering peaks at d = 3.5 and 1.2 nm were observed in the out-of-plane direction. Although we cannot assign these peaks, it was found that similar peaks appeared for all the three **(PDI–PDMS$_m$)$_n$** films (Fig. 6e–g). Based on this fact, a certain long-range order was present for these films, where the periodicity was independent of chain length. We speculate that the packing of PDI molecules is the origin of these scattering peaks. However, the driving force of crystallization may be stronger when long PEG chains were utilized. Thus, crystalline PEG peaks were the dominant feature for the PEG-based polymers.

Intrinsic electron transport property in solid films: microwave-based conductivity evaluation and transient absorption spectroscopy

Strong steady state interaction between PDI chromophores was revealed in **(PDI–PDMS$_m$)$_n$**, while the long-range clear periodic

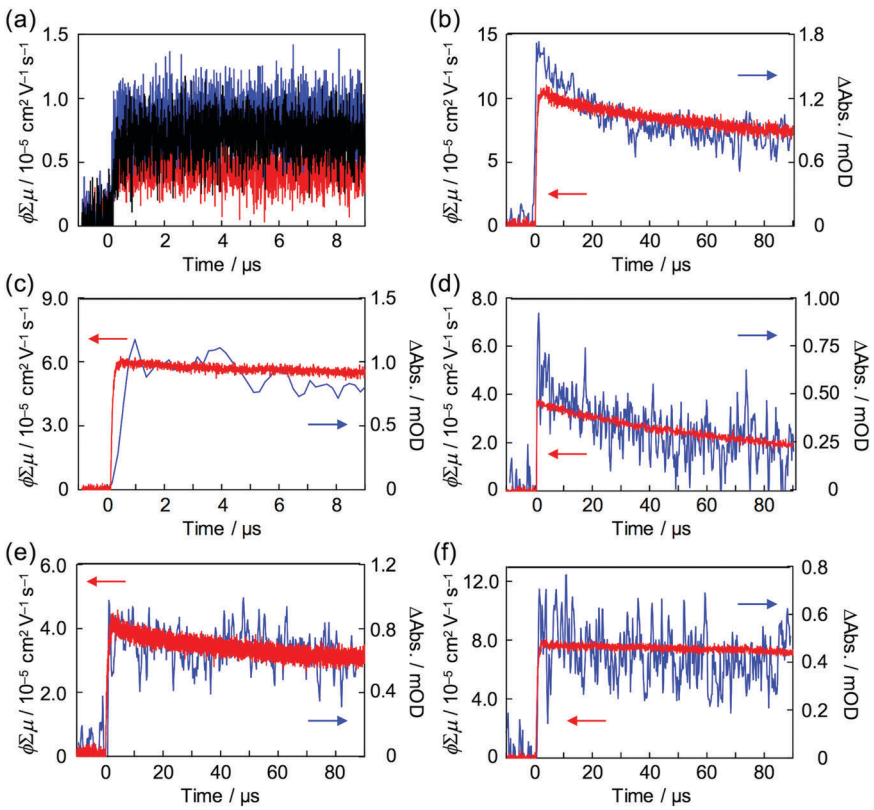

Fig. 7 (a) Kinetic profiles of FP-TRMC observed for dropcast films of **(PDI–PDMS$_{1000}$)$_n$** (red), **(PDI–PDMS$_{2500}$)$_n$** (blue), and **(PDI–PDMS$_{5000}$)$_n$** (black). Kinetic profiles of FP-TRMC (red) and transient absorption spectra at 730 nm (blue) observed for dropcast films of (b) **(PDI–PEG$_{2000}$)$_n$**, (c) **(PDI–PEG$_{6000}$)$_n$**, (d) **(PDI–PPG$_{4000}$)$_n$**, (e) **PDMS$_{2000}$–PDI–PDMS$_{2000}$**, and (f) **PEG$_{2000}$–PDI–PEG$_{2000}$**. The samples were photoexcited at 355 nm with a photon density of 9.1 × 10^{15} cm^{-2} pulse^{-1}.

structure was confirmed in **(PDI–PEG$_m$)$_n$** with almost identical inter-planer distances of 0.34 nm for electron delocalization over the columnar stacking axes.[34,65] Local charge carrier motion has been assessed by combination of time-resolved microwave conductivity (TRMC) measurement and transient absorption spectroscopy (TAS)[31,66,67] to address the question of which is more advantageous for charge carrier transport: stable inter-planer interaction in the steady state or long-range periodicity of π–π stacking with high crystallinity. Except for the **(PDI–PDMS$_m$)$_n$** copolymers, clear conductivity transients in TRMC were observed in the series of copolymers upon photo-irradiation at 355 nm (Fig. 7), where an isolated PDI chromophore exhibits only a slight optical transition dipole and then the light absorption depth profile is almost constant, suppressing the second order recombination kinetics due to the highly concentrated electron–hole pairs around the top surfaces (absorptivity: $\alpha \sim 0.5\ \mu m^{-1}$). This is also supported by the small mismatches of kinetic traces of transient conductivity and radical anions of PDI monitored by TAS at 730 nm[68,69] in the time range of a few μs (Fig. 7b and c) observed in the PDI–PEG systems. Overall, the kinetic traces of both the transient absorption and TRMC measurements are well overlapped in the entire time course to 100 μs, suggesting the conductivity signal clearly originates from the free electrons generated on the PDI chromophores ($PDI^{\bullet -}$). The molar extinction coefficient of $PDI^{\bullet -}$ had been reported as $\varepsilon(PDI^{\bullet -}) = 74\,000\ M^{-1}\ cm^{-1}\ (anions)^{-1}$, allowing the fully-experimental determination of photoionization yield (ϕ) in the copolymer systems upon 355 nm excitation. Since the photoconductivity kinetic traces are normalized by the value of ϕ and given as $\phi\sum\mu$, dividing the value of $(\phi\sum\mu)_{max}$ by ϕ_{max} at the end of the kinetics leads to the local mobility of electrons ($\sum\mu$) in the present system, which is summarized in Table 3. Herein, **(PDI–PEG$_{2000}$)$_n$** marked the highest electron mobility of 0.2 $cm^2\ V^{-1}\ s^{-1}$, while the values of both ϕ and $\phi\sum\mu$ were negligible in **(PDI–PDMS$_m$)$_n$** copolymers. This implies that the steady state π–π inter-molecular interactions cannot overcome the thermal fluctuation of PDMS chains with the higher entropy terms, while the high crystallinity of PEG chains in the copolymer systems assists an effective hopping transport of electrons along the PDI aggregates. For the future design of 'elastic' electronic copolymers with folding–unfolding behaviours, it is presumed to be important to design semi-flexible inter-linking chains with entropy terms between those of the PEG and PDMS chains.

Table 3 Summary of maximum values of $\phi\sum\mu$ in FP-TRMC, ϕ_{max} values from TAS, and calculated $\sum\mu$ values for PDI-based alternating copolymers and reference compounds

Entry	$(\phi\sum\mu)_{max}$[a] / $cm^2\ V^{-1}\ s^{-1}$	ϕ_{max}[b]	$\sum\mu$[c] / $cm^2\ V^{-1}\ s^{-1}$
(PDI–PDMS$_{1000}$)$_n$	0.5×10^{-5}	—[a]	—[a]
(PDI–PDMS$_{2500}$)$_n$	0.8×10^{-5}	—[a]	—[a]
(PDI–PDMS$_{5000}$)$_n$	0.7×10^{-5}	—[a]	—[a]
(PDI–PEG$_{2000}$)$_n$	1.1×10^{-4}	4.6×10^{-4}	0.2
(PDI–PEG$_{6000}$)$_n$	6.0×10^{-5}	9.2×10^{-4}	0.07
(PDI–PPG$_{2000}$)$_n$	2.0×10^{-5}	2.2×10^{-4}	0.1
(PDI–PPG$_{4000}$)$_n$	3.5×10^{-5}	6.3×10^{-5}	0.06
PDMS$_{2000}$–PDI–PDMS$_{2000}$	4.0×10^{-5}	9.0×10^{-5}	0.04
PEG$_{2000}$–PDI–PEG$_{2000}$	8.0×10^{-5}	6.2×10^{-4}	0.1

[a] $(\phi\sum\mu)_{max}$ is a maximum value of the FP-TRMC trace. [b] ϕ_{max} was calculated from the maximum value of ΔO.D. at 730 nm and absorption coefficient of PDI radical anions. [c] $\sum\mu$ was calculated by dividing of the value of $\phi\sum\mu$ by ϕ value picked up at the time where both kinetics are overlapped.

Conclusions

Alternating copolymers of a perylenediimide (PDI) π-system and flexible macromolecular chains such as poly(dimethylsiloxane) (PDMS), poly(ethyleneglycol) (PEG), and poly(propylene glycol) (PPG) were newly synthesized in order to focus on their folding behaviour to construct electron-transporting PDI arrays *via* self-assembly. Due to the highly flexible nature of PDMS chains, PDI–PDMS alternating copolymers showed a distinct folding behaviour in THF solution, which was confirmed by the inter-PDI interactions observed by means of absorption spectroscopy and fluorescence spectroscopy. Inverse distribution of $A^{0\rightarrow0}/A^{0\rightarrow1}$ at around 0.6 as well as excimer formation of PDI–PDMS polymers strongly supported this folding event, whereas PDI–PEG polymers exhibited a weaker tendency of folding and PPG-based ones appeared to be almost dispersed in solution. The effectiveness of alternating copolymer structures was clearly demonstrated by comparing the reference macromonomer compounds of a PDI molecule carrying two PDMS or PEG chains at its termini, where these reference macromolecular compounds showed less inter-PDI interactions in solution. Therefore, it was revealed that the entropic effect of PDMS linkers strongly helps the PDI–PDI interactions in PDI–PDMS polymers. In the solid state, PDI–PDMS polymers afforded broad X-ray diffraction peaks corresponding to inter-plane distances among PDI units, while crystalline peaks of PEG chains appeared for the PDI–PEG polymers. Combination of flash-photolysis microwave conductivity and transient absorption spectroscopy for the solid films dropcast from THF solution disclosed the electron-transporting property for these PDI-based polymers in a fully-experimental and non-contact manner. In contrast to the much smaller conductivity and absorption signals for PDI–PDMS polymers, which indicate the low yields of photoinduced charge generation, PDI–PEG polymers recorded an intrinsic electron mobility of 0.2 $cm^2\ V^{-1}\ s^{-1}$. Although the PDI–PDMS polymers are capable of folding even in diluted solution, long-range crystalline order of PEG chains may be effective in the solid state to align PDI chromophores and eventually provide the higher electron mobility. Selection of chains with appropriate entropy terms between PEG and PDMS chains would also be promising for the progress of foldamer-based soft organic electronics.

Conflicts of interest

The authors declare no conflict of interest.

Acknowledgements

This work was partially supported by the Grant-in-Aid for Scientific Research (No. 26102011, 15K21721, 26249145, and

17H04880) from Japan Society for the Promotion of Science (JSPS) and research grants from the Ogasawara Foundation for the Promotion of Science & Engineering, Tateisi Science and Technology Foundation, the Eno Science Foundation, and Iketani Science and Technology Foundation. The synchrotron radiation experiments were performed at BL44B2 in SPring-8 with the approval of RIKEN (Proposal No. 20160014). GI-XS experiments were conducted in Nagoya University, supported by Nanotechnology Platform Program of MEXT, Japan (Proposal No. S-16-NU-0017). We also acknowledge Prof. Akihiro Ito for the evaluation of absolute photoluminescence quantum yield and DLS measurements for Prof. Kenji Matsuda and Prof. Takashi Hirose in Kyoto University.

Notes and references

1 M. U. Ocheje, B. P. Charron, A. Nyayachavadi and S. Rondeau-Gagné, *Flexible Printed Electron.*, 2017, **2**, 043002.
2 R. Xie, R. H. Colby and E. D. Gomez, *Adv. Electron. Mater.*, 2017, **3**, 1700356.
3 Y. H. Lee, M. Jang, M. Y. Lee, O. Y. Kweon and J. H. Oh, *Chem*, 2017, **3**, 724–763.
4 A. D. Printz and D. J. Lipomi, *Appl. Phys. Rev.*, 2016, **3**, 021302.
5 H.-C. Kim, S.-M. Park and W. D. Hinsberg, *Chem. Rev.*, 2010, **110**, 146–177.
6 H. G. Yoo, M. Byun, C. K. Jeong and K. J. Lee, *Adv. Mater.*, 2015, **27**, 3982–3998.
7 C. Leitold and C. Dellago, *J. Chem. Phys.*, 2014, **141**, 134901.
8 C. K. Ober, J. I. Jin, Q. Zhou and R. W. Lenz, Liquid crystal polymers with flexible spacers in the main chain, in *Liquid Crystal Polymers I. Advances in Polymer Science*, ed. N. A. Platé, Springer, Berlin, Heidelberg, 1984, vol. 59.
9 C. Ober, R. W. Lenz, G. Galli and E. Chiellini, *Macromolecules*, 1983, **16**, 1034–1036.
10 J. S. Moore and S. I. Stupp, *Macromolecules*, 1987, **20**, 282–293.
11 S. W. Kantor, T.-C. Sung and E. D. T. Atkins, *Macromolecules*, 1992, **25**, 2789–2795.
12 Z. R. Wagner, T. K. Roenigk and F. E. Goodson, *Macromolecules*, 2001, **34**, 5740–5743.
13 M. T. Hargadon, E. A. Davey, T. B. Mcintyre, D. Gnanamgari, C. M. Wynne, R. C. Swift, J. R. Zimbalist, B. L. Fredericks, A. J. Nicastro and F. E. Goodson, *Macromolecules*, 2008, **41**, 741–750.
14 J. A. Osaheni and S. A. Jenekhe, *J. Am. Chem. Soc.*, 1995, **117**, 7389–7398.
15 Z. Yang, F. E. Karasz and D. C. Morton, *J. Chem. Phys.*, 1993, **74**, 3584–3586.
16 X. Zhu, M. C. Traub, D. A. Vanden Bout and K. N. Plunkett, *Macromolecules*, 2012, **45**, 5051–5057.
17 M. C. Traub, K. H. Dubay, S. E. Ingle, X. Zhu, K. N. Plunkett, D. R. Reichman and D. A. V. Bout, *J. Phys. Chem. Lett.*, 2013, **4**, 2520–2524.
18 J. M. Lucas, J. A. Labastide, L. Wei, J. S. Tinkham, M. D. Barnes and P. M. Lahti, *J. Phys. Chem. A*, 2015, **119**, 8010–8020.
19 D. H. Appella, L. A. Christianson, I. L. Karle, D. R. Powell and S. H. Gellman, *J. Am. Chem. Soc.*, 1996, **118**, 13071–13072.
20 S. H. Gellman, *Acc. Chem. Res.*, 1998, **31**, 173–180.
21 J. C. Nelson, J. G. Saven, J. S. Moore and P. G. Wolynes, *Science*, 1997, **277**, 1793–1796.
22 D. J. Hill, M. J. Mio, R. B. Prince, T. S. Hughes and J. S. Moore, *Chem. Rev.*, 2001, **101**, 3893–4011.
23 T. Muraoka, T. Shima, T. Hamada, M. Morita, M. Takagi and K. Kinbara, *Chem. Commun.*, 2011, **47**, 194–196.
24 T. Muraoka and K. Kinbara, *Chem. Commun.*, 2016, **52**, 2667–2678.
25 Y. Zheng, H. Zhou, D. Liu, G. Floudas, M. Wagner, K. Koynov, M. Mezger, H. J. Butt and T. Ikeda, *Angew. Chem., Int. Ed.*, 2013, **52**, 4845–4848.
26 T. Ikeda, *Langmuir*, 2015, **31**, 667–673.
27 M. Vybornyi, A. Rudnev and R. Häner, *Chem. Mater.*, 2015, **27**, 1426–1431.
28 T. Mondal, K. Dan, J. Deb, S. S. Jana and S. Ghosh, *Langmuir*, 2013, **29**, 6746–6753.
29 T. Mondal, T. Sakurai, S. Yoneda, S. Seki and S. Ghosh, *Macromolecules*, 2015, **48**, 879–888.
30 T. Ikeda, H. Tamura, T. Sakurai and S. Seki, *Nanoscale*, 2016, **8**, 14673–14681.
31 S. Seki, A. Saeki, T. Sakurai and D. Sakamaki, *Phys. Chem. Chem. Phys.*, 2014, **16**, 11093–11113.
32 A. Saeki, Y. Koizumi, T. Aida and S. Seki, *Acc. Chem. Res.*, 2012, **45**, 1193–1202.
33 F. C. Grozema and L. D. A. Siebbeles, *J. Phys. Chem. Lett.*, 2011, **2**, 2951–2958.
34 F. Würthner, C. R. Saha-Möller, B. Fimmel, S. Ogi, P. Leowanawat and D. Schmidt, *Chem. Rev.*, 2016, **116**, 962–1052.
35 E. E. Neuteboom, R. A. J. Janssen and E. W. Meijer, *Synth. Met.*, 2001, **121**, 1283–1284.
36 E. E. Neuteboom, S. C. J. Meskers, E. W. Meijer and R. A. J. Janssen, *Macromol. Chem. Phys.*, 2004, **205**, 217–222.
37 S. K. Nisha and S. K. Asha, *ACS Appl. Mater. Interfaces*, 2014, **6**, 12457–12466.
38 Y. Liang, D. Wang, Y. Wu, Q. Lai, L. Xue and S. Feng, *Appl. Surf. Sci.*, 2011, **257**, 10576–10580.
39 W. Wang, L. S. Li, G. Helms, H. H. Zhou and A. D. Q. Li, *J. Am. Chem. Soc.*, 2003, **125**, 1120–1121.
40 W. Wang, J. J. Han, L.-Q. Wang, L.-S. Li, W. J. Shaw and A. D. Q. Li, *Nano Lett.*, 2003, **2**, 455–458.
41 A. D. Q. Li, W. Wang and L. Q. Wang, *Chem. – Eur. J.*, 2003, **9**, 4594–4601.
42 A. D. Shaller, W. Wang, A. Li, G. Moyna, J. J. Han, G. L. Helms and A. D. Q. Li, *Chem. – Eur. J.*, 2011, **17**, 8350–8362.
43 K. Kato and H. Tanaka, *Adv. Phys.: X*, 2016, **1**, 55–80.
44 M. Sano, S. Nakamura, M. Hara, S. Nagano, Y. Shinohara, Y. Amemiya and T. Seki, *Macromolecules*, 2014, **47**, 7178–7186.
45 C. Aguilera, J. Bartulin, B. Hisgen and H. Ringsdorf, *Makromol. Chem.*, 1983, **262**, 253–262.
46 A. B. Samui, S. Pandey and S. P. Mishra, *RSC Adv.*, 2015, **5**, 68351–68355.
47 M. Zhao, K. Hashimoto and K. Tajima, *Synth. Met.*, 2013, **175**, 9–14.
48 K. L. Geisinger and G. V. Gibbs, *Phys. Chem. Miner.*, 1983, **7**, 204–210.
49 P. Buckley and P. A. Giguère, *Can. J. Chem.*, 1967, **45**, 397–407.

50 H. Langhals and R. Ismael, *Eur. J. Org. Chem.*, 1998, 1915–1917.
51 J. Sung, A. Nowak-Król, F. Schlosser, B. Fimmel, W. Kim, D. Kim and F. Würthner, *J. Am. Chem. Soc.*, 2016, **138**, 9029–9032.
52 S. Yagai, T. Seki, T. Karatsu, A. Kitamura and F. Würthner, *Angew. Chem., Int. Ed.*, 2008, **47**, 3367–3371.
53 S. Ghosh, X. Q. Li, V. Stepanenko and F. Würthner, *Chem. – Eur. J.*, 2008, **14**, 11343–11357.
54 M. Kasha, H. R. Rawls and M. Ashraf El-Bayoumi, *Pure Appl. Chem.*, 1965, **11**, 371–392.
55 W. E. Ford, *J. Photochem.*, 1987, **37**, 189–204.
56 H. Langhals, *Helv. Chim. Acta*, 2005, **88**, 1309.
57 Z. Chen, B. Fimmel and B. F. Würthner, *Org. Biomol. Chem.*, 2012, **10**, 5845–5855.
58 The possibility of concentration changes upon heating was discussed in detail in the ESI.† The small values of volume expansion coefficients a $[=(1/V_m)(dV_m/dT)]$ ranging in 0.9–1.2 $\times$ 10^{-3} K^{-1} for ethers, the presence of isosbestic points in absorption spectra upon heating, and the fact of no distinct change for the $CHCl_3$ solution case are the discussed points.
59 D. Veldman, S. M. A. Chopin, S. C. J. Meskers, M. M. Groeneveld, R. M. Williams and R. A. J. Janssen, *J. Phys. Chem. A*, 2008, **112**, 5846–5857.
60 M. Sadrai, L. Hadel, R. R. Sauers, S. Husain, K. Krogh-Jespersen, J. D. Westbrook and G. R. Bird, *J. Phys. Chem.*, 1992, **96**, 7988–7996.
61 S. J. Clarson, K. Dodgson and J. A. Semlyen, *Polymer*, 1985, **26**, 930–934.
62 P. Tormala, *Eur. Polym. J.*, 1974, **10**, 519–521.
63 G. P. Johari, A. Hallbrucker and E. Mayer, *J. Polym. Sci., Part B: Polym. Phys.*, 1988, **26**, 1923–1930.
64 T. Sakurai, Y. Tsutsui, K. Kato, M. Takata and S. Seki, *J. Mater. Chem. C*, 2016, **4**, 1490–1496.
65 V. Percec, H. J. Sun, P. Leowanawat, M. Peterca, R. Graf, H. W. Spiess, X. Zeng, G. Ungar and P. A. Heiney, *J. Am. Chem. Soc.*, 2013, **135**, 4129–4148.
66 A. Saeki, S. Seki, Y. Koizumi and S. Tagawa, *J. Photochem. Photobiol., A*, 2007, **186**, 158–165.
67 S. Yagai, M. Usui, T. Seki, H. Murayama, Y. Kikkawa, S. Uemura, T. Karatsu, A. Kitamura, A. Asano and S. Seki, *J. Am. Chem. Soc.*, 2012, **134**, 7983–7994.
68 W. E. Ford, H. Hiratsuka and P. V. Kamat, *J. Phys. Chem.*, 1989, **93**, 6692–6696.
69 D. Gosztola, M. P. Niemczyk, W. Svec, A. S. Lukas and M. R. Wasielewski, *J. Phys. Chem. A*, 2000, **104**, 6545–6551.